

21.2 On the Need for Perturbed LBCs in Limited-Area Ensemble Forecasts

Paul Nutter^{1, *} †, Ming Xue¹, and David Stensrud²

¹School of Meteorology, and
Center for Analysis and Prediction of Storms
University of Oklahoma, Norman, Oklahoma

²National Severe Storms Laboratory, Norman, Oklahoma

1. Introduction

Nutter (2003) showed that the use of coarsely resolved and/or temporally interpolated lateral boundary conditions (LBCs) is sufficient to cause underdispersive limited area model (LAM) ensemble forecasts. The effect is present in all typical modeling systems using “one-way” LBC forcing and suggests the need to apply statistically consistent, finescale LBC perturbations at every time step throughout the LAM simulations. In this paper, we present a method for introducing LBC perturbations that is designed specifically to help restore the loss of LAM ensemble dispersion using a simplified model system.

The use of coarsely resolved and temporally interpolated LBCs restricts small scale error growth in LAMs because of the LBC “sweeping” effects that were documented by Nutter et al. (2004) using a carefully controlled approach. This limitation of LAMs has important consequences because it artificially inflates estimates of predictability limits which, in turn, decreases forecast uncertainty. The LBC sweeping mechanism associated with coarsely resolved LBCs has been considered previously by a number of authors including Errico and Baumhefner (1987), Vukicevic and Errico (1990), Paegle et al. (1997), Warner et al. (1997), Hou et al. (2001), and De Elía and Laprise (2002). Nutter et al. (2004) additionally considered error growth constraints introduced by temporal interpolation between relatively infrequent LBC updates and extended the analysis to quantify the impact on LAM ensemble dispersion. They concluded that it is difficult to construct an efficacious LAM ensemble system unless these LBC constraints on error growth are relaxed. To help im-

prove the design of LAM ensemble systems, LBC perturbations are introduced in this paper to help counter LBC sweeping effects by creating a statistically consistent source of error growth along the lateral boundaries. The LBC perturbations are designed to amplify with time while coherently propagating into the domain. The perturbations are shown to help restore small-scale error growth that would otherwise be swept away through the downstream boundary.

The application of LBC perturbations described herein has not previously been attempted to the authors’ knowledge. The method goes beyond the common practice of using an ensemble of unique LBCs provided by individual members of an external model ensemble. Earlier results by Nutter et al. (2004) showed that an ensemble of LBCs does not mitigate the LBC constraint on error growth at small scales because the LBCs are still coarsely resolved in both space and time. Hence, the LBC perturbation method described here is superposed upon the full set of LBCs originating as output from an ensemble of external model forecasts.

We begin in section two with a review of statistical measures used by Nutter et al. (2004) because the same measures are applied herein to quantify ensemble performance. In section three, we review the simplified model system used by Nutter et al. (2004) that is designed to isolate and control LBC errors. An example LAM ensemble simulation obtained from this model is presented in section four to provide a basis for evaluating the impact of LBC perturbations. Composition of the LBC perturbations is detailed in section five. Statistical results shown in section six

* *Current affiliation:* Cooperative Institute for Mesoscale Meteorological Studies, University of Oklahoma, Norman, Oklahoma

† *Corresponding author email:* pnutter@ou.edu.

quantify how well the perturbations help restore LAM ensemble dispersion. Concluding remarks address the need for additional development before LBC perturbations can be applied in operational settings.

2. Ensemble Statistics

The ensemble statistics introduced by Nutter (2003) and Nutter et al. (2004) are reviewed here for completeness. Suppose \mathbf{x}_i is a vector field defined on a p -element grid, representing forecasts or analyses obtained from an N -member ensemble, where $i = 1, \dots, N$. The ensemble mean (a p -element column vector) is defined

$$\bar{\mathbf{x}} = \frac{1}{N} \sum_{i=1}^N \mathbf{x}_i. \quad (1)$$

The scalar spatial mean for the i th ensemble member is given by

$$\langle \mathbf{x}_i \rangle = \frac{1}{p} \sum_{k=1}^p \mathbf{x}_{i,k} = \frac{1}{p} \mathbf{1} \cdot \mathbf{x}_i, \quad (2)$$

where $\mathbf{1}$ is a p -element vector of ones. A useful norm representing the average sum of squares (dot product) over the grid is

$$\|\mathbf{x}_i\|^2 = \frac{1}{p} \mathbf{x}_i \cdot \mathbf{x}_i = \frac{1}{p} \sum_{k=1}^p \mathbf{x}_{i,k}^2. \quad (3)$$

Henceforth, let $\mathbf{f}_i(t)$ denote individual forecast vectors from the ensemble and $\mathbf{a}(t)$ represent the analysis vector corresponding to each forecast. Note that there is only one analysis vector for each time so that $\mathbf{a}_i(t) = \mathbf{a}(t) = \bar{\mathbf{a}}$. The forecasts and analysis are functions of time, but we will henceforth drop the (t) notation. These definitions are applicable for gridded fields on both global (periodic, or laterally unbounded) and limited-area domains unless specified otherwise.

Using the norms defined above, the ensemble dispersion (D^2), the ensemble mean square error (S^2), and the total biased error variance (σ^2) are defined as follows:

$$D^2 = \frac{1}{N} \sum_{i=1}^N \|\mathbf{f}_i - \bar{\mathbf{f}}\|^2, \quad (4)$$

$$S^2 = \frac{1}{N} \sum_{i=1}^N \|\mathbf{f}_i - \mathbf{a}\|^2 = D^2 + \|\bar{\mathbf{f}} - \mathbf{a}\|^2, \quad (5)$$

$$\sigma^2 = \frac{1}{N} \sum_{i=1}^N \|(\mathbf{f}_i - \mathbf{a}_i) - \langle \mathbf{f}_i - \mathbf{a}_i \rangle \mathbf{1}\|^2. \quad (6)$$

The total biased error variance (σ^2) may be obtained equivalently in spectral form as (Errico, 1985)

$$\sigma^2 = \frac{1}{N} \sum_{i=1}^N \sum_{\kappa=1}^{K-1} 2 |F_i(\kappa)|^2, \quad (7)$$

where $F_i(\kappa)$ is the discrete Fourier transform of $\mathbf{f}_i - \mathbf{a}$ and $\kappa = 1, \dots, K - 1$ are the set of Nyquist resolved wavenumbers on the grid (Errico, 1985). In this form, error variances may be computed individually for specific wavenumbers, or accumulated over a range of scales.

One-dimensional spectra are obtained from the two-dimensional fields using the procedure described by Errico (1985). Specifically, linear trends are first removed from each row and column of the two-dimensional grid. Then variance spectra are obtained by summing the magnitude of Fourier coefficients within annular rings in wavenumber space. Refer to Errico (1985) and Nutter (2003) for details.

A key aspect of this work is to study the impact of scale deficient lateral boundary conditions on LAM ensemble dispersion. To study this effect as a function of wavelength, we can link ensemble dispersion to the spectral decomposition of total error variance using the relation

$$D^2 = \sigma^2 + \frac{1}{N} \sum_{i=1}^N (\langle \mathbf{f}_i \rangle - \langle \mathbf{a} \rangle)^2 - \|\bar{\mathbf{f}} - \mathbf{a}\|^2, \quad (8)$$

which is derived by Nutter et al. (2004). Using the spectral variance from (7), Eq. 8 shows that ensemble dispersion is determined by the accumulated contributions to error variance at all resolved wavelengths, the ensemble mean square spatial error (sme)², and a reduction from the squared error of the ensemble mean (eme)². This expression will be applied in section six to evaluate the impact of perturbed LBCs on ensemble dispersion by comparing the magnitudes of each term obtained for both global and LAM simulations.

The latter two terms in (8) cannot be decomposed in a simple way to reveal their contributions to D^2 at different scales. However, if these terms are nearly the same for both global and LAM simulations, then their contributions to D^2 are negated under comparison. Under this condition, the direct spectral relation between error variance and ensemble dispersion is maintained. In the perfect model simulations conducted for this work, the ensembles are unbiased and the spatial error term is negligible on large domains. However, on small domains, the spectral calculation of ensemble dispersion could

become distorted because of phase errors introduced by upscale perturbation growth. The ensemble bias term could become large in practical application due to model deficiencies. However, ensembles can be calibrated to remove such biases (Hamill and Colucci, 1997; Hamill, 2001).

The climatological variance provides a natural standard of forecast skill since the theoretical upper bound for S^2 and σ^2 at error saturation is twice the climate variance of analyses (Leith, 1974; Nutter, 2003). To normalize the statistics in this work, let $F_j^a(\kappa)$ be the coefficients obtained from the discrete Fourier transform of the analysis field \mathbf{a}_j , where $j = 1, \dots, M$ and M denotes the number of independent cases. Then, following (7), the fraction of total variance contributed by wavenumber(s) between k_1 and k_2 ($1 \leq k_1 \leq k_2 \leq K - 1$) averaged over all M cases is determined using

$$\tilde{\eta}_{\mathbf{a}}(\kappa) = \frac{\frac{1}{M} \sum_{j=1}^M \frac{1}{N} \sum_{i=1}^N \sum_{\kappa=k_1}^{k_2} 2 |F_i(\kappa)|^2}{\frac{1}{M} \sum_{j=1}^M \sum_{\kappa=k_1}^{k_2} 2 |F_j^a(\kappa)|^2}. \quad (9)$$

The normalization applies equally to all wavenumbers, and has a theoretical maximum value of two.

3. Numerical model and its configurations

Numerical experiments are conducted using a single-level modified barotropic vorticity channel model. The model is configured specifically to isolate the effects of LBCs on LAM ensemble dispersion while avoiding analysis and model system errors. Although simplified, the model remains nonlinear, dispersive, and sensitive to initial condition (IC) perturbations.

The model is based on a parameterized version of the quasi-geostrophic potential vorticity equation (Holton, 1979, Sec. 8.4.2). Hence, we call it the parameterized potential vorticity (PPV) model. Let $\xi \equiv \zeta - \lambda^2 \psi$ define the parameterized potential vorticity, where ζ denotes relative vorticity, ψ is the streamfunction, and λ is the inverse of the Rossby radius of deformation specified so that $\lambda^{-1} = 1414.2$ km. If we apply this approximation to the quasi-geostrophic potential vorticity equation and introduce a 4th-order numerical diffusion term having an eddy diffusion coefficient ν , we obtain the PPV model

$$\frac{\partial \xi}{\partial t} = \frac{\partial \psi}{\partial y} \frac{\partial \xi}{\partial x} - \frac{\partial \psi}{\partial x} \left(\frac{\partial \xi}{\partial y} + \beta \right) - \nu \nabla^2 \xi, \quad (10)$$

where β is the meridional gradient of Earth's vorticity evaluated at 45 degrees north latitude. The model's numerics are described fully in Nutter (2003) and summarized in Nutter et al. (2004).

PPV model simulations are run with "global" and limited-domain configurations. Both configurations operate with the same time step and with 25 km grid spacing to avoid the impact of numerical discretization errors when comparing simulations to a model-generated truth. The global model configuration is a zonally periodic channel domain dimensioned 18000 km from west to east and 6000 km from south to north. Four different LAM domains are defined as subsets of the periodic channel domain [see Fig. 1 in Nutter et al. (2004)]. The largest nested-domain is 6000 km², the medium-sized domain is 3000 km², and the two smallest domains are 1500 km². One of the small domains is displaced southward in the channel relative to the centralized position of the others to evaluate error growth in a less unstable part of the flow.

The LAM simulations are configured using "one-way" Dirichlet boundary conditions for ψ and ξ obtained from subsets of the global model simulations. The one-way LBC scheme in the LAM simulations applies a 7-point peripheral relaxation zone (Davies, 1976, 1983). LBCs are obtained by linearly interpolating between subsets of the global simulations at 1, 3, and 6-hourly intervals. Coarsely resolved LBC fields are generated by applying a low-pass spatial filter to fields from global model simulations running at the same resolution as the LAM. The low-pass filter is a Fourier transform procedure (Errico, 1985; Laprise et al., 2000; Nutter, 2003) that removes completely all wavelengths shorter than 150 km while perfectly retaining the amplitudes of wavelengths longer than 450 km. The filtering process preserves the accuracy of large scale motions while removing those which would not be present on a grid having three times less spatial resolution as the LAM grid. This analysis procedure is similar to that used most recently by Laprise et al. (2000) and De Elía and Laprise (2002).

A model-generated climatology of 100 independent cases is used to obtain ICs and perturbations for ensembles following the method used by Schubert and Suarez (1989). Specifically, two unique states are randomly selected from the model's set of climatological states. Perturbations are then formed by scaling the difference between the two samples by a factor of 0.10. Finally, the perturbation field is added to an IC field represented by another climatological state. This perturbation procedure is repeated ten times for a given initial field to create the starting conditions for 10-member ensemble simulations. One-hundred independent 10-member ensemble simulations are constructed by assigning perturbations to ICs given by each of the available

climatological cases.

4. Example Simulation - Unperturbed LBCs

An example simulation is reproduced from Nutter et al. (2004) to show the effects of coarsely resolved and temporally interpolated LBCs on ensemble dispersion and to provide a basis for later comparison against the same case run using LBC perturbations. The example case is run as a LAM ensemble configured with 3-hourly updated and low-pass filtered (coarsely-resolved) LBCs run on the medium domain. The ICs and LBCs for individual members are obtained as direct subsets of the corresponding global ensemble members, so an unperturbed “ensemble of LBCs” has been applied.

To visualize the documented loss of ensemble dispersion due to LBC filtering effects, the following loss ratio is defined at each grid point p in the domain:

$$1 - \frac{d_p^2(\text{global})}{d_p^2(\text{LAM})} \quad (11)$$

where d_p^2 is the local dispersion defined similar to (4) except it is not averaged over the domain. If this loss ratio is locally negative, then the LAM ensemble has less dispersion than the global ensemble at that grid point.

The example LAM ensemble and its dispersion loss ratio is shown in Fig. 1. At the initial time (panel a), regions of increased and decreased vorticity dispersion relative to the global ensemble appear evenly distributed and similar in magnitude since the loss ratio is near zero everywhere. After 12 hours have elapsed (panel b), regions showing strong reductions of dispersion appear along the upstream side of the domain. At the same time, the dispersion loss ratio remains evenly distributed and near zero within the downstream portion of the domain. The reductions near the upstream boundary is attributed to the spatial and temporal filtering effects associated with the use of coarsely-resolved and temporally-interpolated LBCs. The area impacted by loss of dispersion grows with time as LBC errors sweep through the domain from west to east. Locally, the LAM ensemble dispersion loss ratio shows reductions of a factor of eight or larger.

5. LBC perturbations

Sufficient background information has been given to develop and apply LBC perturbations to the LAM ensemble simulations. The general procedure for im-

plementing LBC perturbations at each time step is as follows (details to follow). A two-dimensional perturbation field is generated on the LAM grid using inverse Fourier transforms. The perturbation field has zero mean and is periodic in both x - and y -directions. The LBC perturbation field is initialized by assigning random phase angles to each wavenumber. Amplitudes of the perturbations are determined by the loss of error variance at specific wavelengths due to LBC effects. Once initialized, the field is translated at the Rossby phase speed for each wavenumber so that perturbations passing through the lateral boundary remain coherent in both space and time. Perturbation amplitudes increase with time based on the amount of error variance needed to restore the portion lost due to LBC sweeping. After the perturbation field is constructed, it is added to the spatially and temporally interpolated LBC field given by subsets of an external model simulation. The perturbed LBC field is then blended with the LAM solution only within a peripheral wave relaxation zone at each time step.

a. Implementation

i. Phase angle form of Fourier series

The net effect of using coarsely resolved and temporally interpolated LBCs is a loss of variance at small scales, and hence, a reduction in the total biased error variance (Nutter et al., 2004). The total biased error variance (Eq. 7) is computed using one-dimensional spectra as described in section two. The error variance calculations retain only wave amplitudes for isotropic wavenumbers and are averaged over many independent cases. The phase angle form of the Fourier series (e.g. Walker, 1988) is most compatible with this statistical framework and is used to synthesize random fields having predetermined error variance spectra.

Consider the Fourier series expansion of a one-dimensional periodic function $f(x) = f(x + L)$:

$$f(x) = a_0 + \sum_{k=1}^{\infty} [a_k \cos(2\pi kx/L) + b_k \sin(2\pi kx/L)], \quad (12)$$

where a_k and b_k are real amplitude coefficients. The phase-angle form of the Fourier series is obtained by letting $a_k = c_k \cos(-\theta_k)$ and $b_k = c_k \sin(-\theta_k)$, where $c_k = \sqrt{a_k^2 + b_k^2}$ and θ_k is the phase angle for wavenumber k . Apply these definitions for a_k and b_k in (12) and manipulate so that

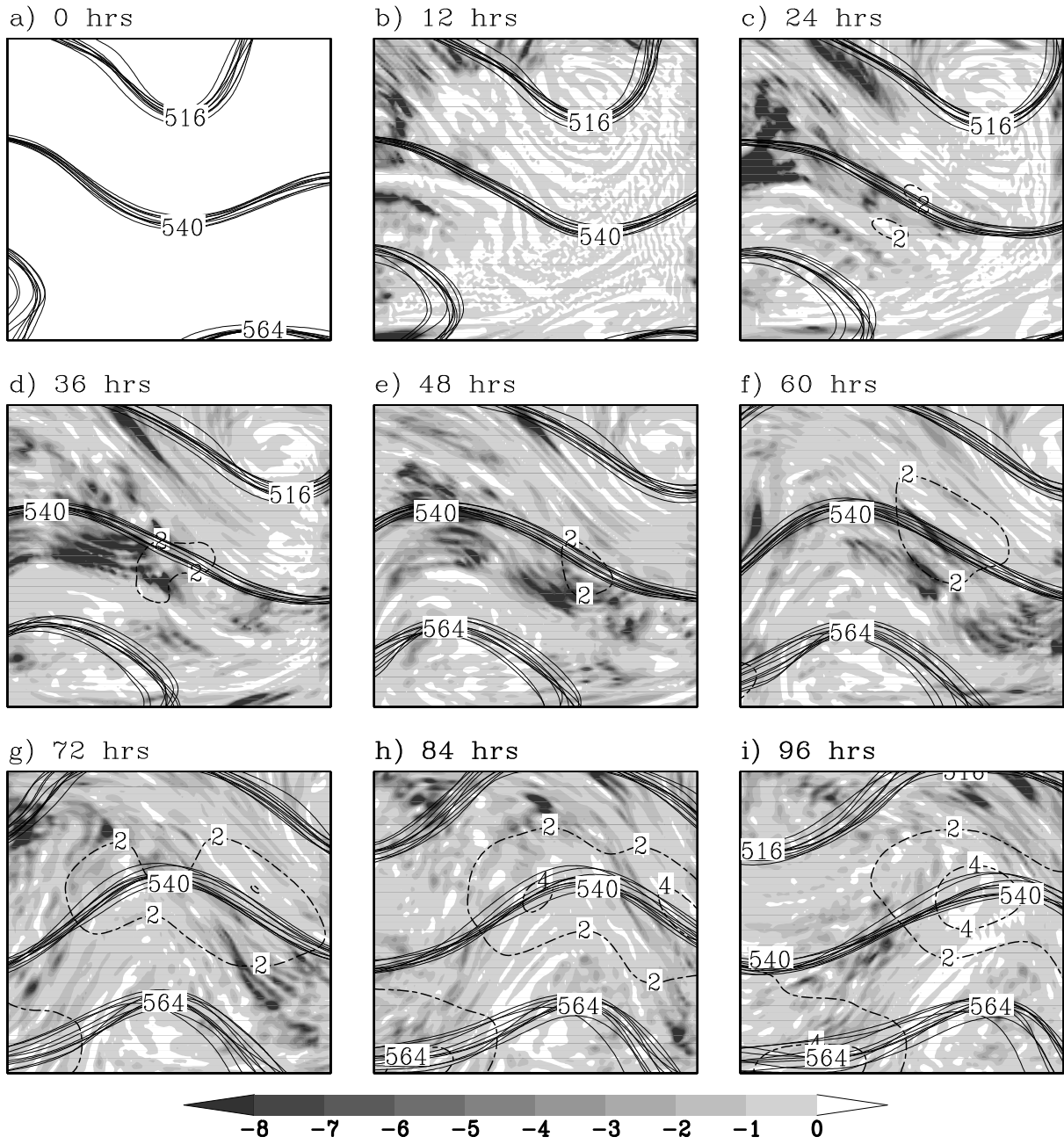


Figure 1: Example case run on the medium domain with 3-hourly updated, low-pass filtered LBCs. A “spaghetti” plot drawn with solid black lines shows the $(516, 540, 564) \times 10^6 \text{ m}^2 \text{ s}^{-1}$ streamlines from each of the 10 LAM ensemble members. Reduction of vorticity dispersion (Eq. 11) is shaded, while streamfunction dispersion is shown with dashed contours at $2 \times 10^{12} \text{ m}^4 \text{ s}^{-2}$ intervals.

$$f(x) = a_0 + \frac{1}{2} \sum_{k=1}^{\infty} \left[c_k e^{i\theta_k} e^{i(2\pi kx/L)} \right] + \frac{1}{2} \sum_{k=1}^{\infty} \left[c_k e^{-i\theta_k} e^{-i(2\pi kx/L)} \right]. \quad (13)$$

Equation (13) shows that a periodic function can be synthesized simply by specifying a real amplitude coefficient (c_k) and phase angle (θ_k) for each wavenumber k . This form is useful because the one-dimensional variance spectra retain only the magnitudes of complex Fourier coefficients. The phase angles remain unknown but may be specified randomly.

Fast Fourier transform (FFT) algorithms use the complex form of the Fourier series. To convert (13) to the more useful complex form, introduce complex Fourier coefficients

$$F(0) = a_0,$$

$$F(k) = \frac{1}{2} c_k e^{i\theta_k} = \frac{1}{2} (a_k - ib_k),$$

$$F(-k) = \frac{1}{2} c_k e^{-i\theta_k} = \frac{1}{2} (a_k + ib_k).$$

Apply these coefficients in (13) so that

$$f(x) = F(0) + \sum_{k=1}^{\infty} \left[F(k) e^{2\pi i k x / L} \right] + \sum_{k=1}^{\infty} \left[F(-k) e^{-2\pi i k x / L} \right]$$

$$f(x) = \sum_{k=0}^{\infty} F(k) e^{2\pi i k x / L} + \sum_{k=-1}^{-\infty} F(k) e^{2\pi i k x / L}$$

$$f(x) = \sum_{k=-\infty}^{\infty} F(k) e^{2\pi i k x / L}. \quad (14)$$

The extension of Eqs. (12) to (14) into their two-dimensional forms is not difficult but involves many additional terms. While details of the derivation are omitted (see Walker, 1988), the complex form of the Fourier series for a two-dimensional periodic field $f(x, y) = f(x + L_x, y + L_y)$ is

$$f(x, y) = \sum_{k=-\infty}^{\infty} \sum_{l=-\infty}^{\infty} F(k, l) \exp[2\pi i (kx/L_x + ly/L_y)]. \quad (15)$$

The discrete Fourier series used for the calculations is

$$f(x, y) \simeq \sum_{k=-N_x/2+1}^{N_x/2} \sum_{l=-N_y/2+1}^{N_y/2} F(k, l) \exp[2\pi i (kx/L_x + ly/L_y)], \quad (16)$$

where $x = (k + N_x/2 + 1)\Delta x$ and $y = (l + N_y/2 + 1)\Delta y$. Even integers N_x and N_y denote the number of grid points along each dimension of the domain. In practice, Fourier series approximation of real fields makes use of complex conjugate symmetries so that the negative l wavenumbers are omitted (Press et al., 1996).

Equation (17) can be used to synthesize a field having pre-determined variance spectra $|F'(k, l)|^2$ and random phase angles $\theta_{k,l}$ by specifying

$$F(k, l) = \sqrt{\frac{|F'(k, l)|^2}{2}} (\cos \theta_{k,l} + i \sin \theta_{k,l}), \quad (17)$$

except the factor of one-half is omitted for $k = 0$ and $k = N_x/2$. This factor is required since error variance spectra obtained previously using FFT algorithms were multiplied by two because of the complex conjugate symmetry in transforms of real data.

ii. Amplitude of Perturbations

Amplitudes of the LBC perturbations are determined by the pre-determined loss of error variance at specific wavelengths due to LBC effects (Nutter et al., 2004). Thus, if σ_{κ}^2 denotes the one-dimensional error variance spectra obtained from previous global and LAM simulations, amplitudes of the perturbation spectra are determined using (17) with

$$|F'(k, l)|^2 = \sigma_{\kappa}^2(\text{global}) - \sigma_{\kappa}^2(\text{LAM}), \quad (18)$$

where $\kappa = \sqrt{k^2 + l^2}$. The perturbation spectra are distributed equally among all the wavenumber pairs (k, l) contained within each annular wavenumber ring $\aleph(\kappa) \pm (1/2)\delta\kappa$, where \aleph denotes nearest integer. Variances are set to zero for wavenumber pairs where κ exceeds that of the smallest resolved wavelength since these were not accumulated in the one-dimensional spectra. Furthermore, negative values of $|F'(k, l)|^2$ are set to zero because, in this case, the error variance in the LAM simulations already exceeds that of the global simulations.

Results in Fig. 2 show $|F'(k, l)|^2$ obtained for the LAM ensemble configuration having 3-hourly updated, low-pass filtered LBCs. Given these difference spectra, amplitudes of the LBC perturbation

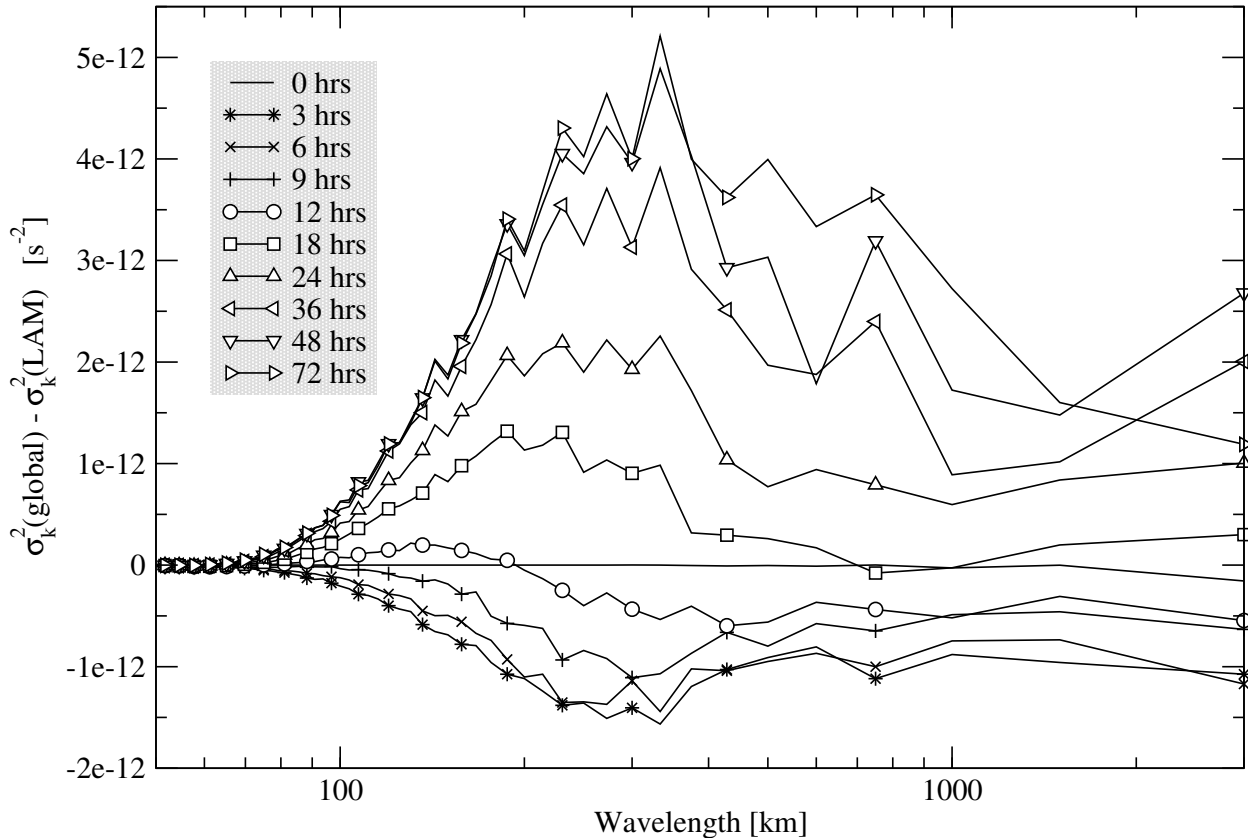


Figure 2: Difference in error variance spectra between global ensemble simulations and LAM ensemble simulations having 3-hourly updated, low-pass filtered LBCs.

field are set to zero for about the first 12 hours, depending on wavelength. The amplitude of the perturbation is greatest at wavelengths between about 100 and 1000 km. Indeed, these are the scales that were most strongly effected by the filtering effects associated with spatial and temporal filtering of LBCs (Nutter et al., 2004). Difference spectra are not shown beyond 72 hours because there is minimal additional growth beyond this time. The LBC perturbation field constructed using the difference spectra in Fig. 2 begin with zero amplitude, then begin to grow after about 12 hours until reaching a nearly constant value around 72 hours.

The difference spectra for these simulations were computed each hour. These spectra were interpolated linearly in time before generating LBC perturbation fields at every 7.5-minute time step of the PPV model. Temporal interpolation of the spectra before generating the perturbation field does not reduce small-scale variance as does interpolation between external LBC fields. Furthermore, temporal changes in the difference spectra are small since

statistics were obtained as averages over 100 cases. In practical applications, data will not be available hourly, perhaps only every 3, or 6 hours. A possible approach for these scenarios is to fit analytic curves to the set of difference spectra (e.g. Lorenz, 1982; Dalcher and Kalnay, 1987; Schubert and Suarez, 1989; Stroe and Royer, 1993; Reynolds et al., 1994; De Elía and Laprise, 2002). Attempts were made to fit such curves here, but it was difficult to obtain parameters that produced accurate fits across all scales of motion. This is an issue that should be addressed further with application to more complex atmospheric LAMs.

iii. Translating the Perturbation Field

The perturbation field is initialized by specifying uniform random phase angles $0 \leq \theta_{k,l} \leq 2\pi$ in (17). Once initialized, the phase angles are stored and incremented at each time step to cause a translation of the perturbation field when it is synthesized using (17). This translation is important for providing

temporally and spatially coherent wave structures as they pass through the lateral boundary. The field is translated at some characteristic speed c_κ by incrementing the phase angles such that

$$\theta_{k,l}(t + \Delta t) = \theta_{k,l}(t) + \kappa c_\kappa \Delta t, \quad (19)$$

where again, $\kappa = \sqrt{k^2 + l^2}$.

An appropriate choice of translation speed for this work is the Rossby phase speed. Since the available error variance spectra are one-dimensional, we use the isotropic, or uni-directional phase speed

$$c_\kappa = (U_0 k - \beta k / \kappa^2) / \kappa, \quad (20)$$

where U_0 is the base state zonal flow speed. Rossby phase speeds calculated using specified PPV model constants are less than 12 ms^{-1} . The x -component of group velocity remains near 12 ms^{-1} while the y -component of group velocity is generally less than 0.001 ms^{-1} . Thus, the entire perturbation field translates from west to east at about 12 ms^{-1} . Other choices for the translation speed could be more appropriate in applications using full primitive equation models. This question remains beyond the scope of the present study.

b. Example Simulation with Perturbed LBCs

An example perturbation vorticity field (ζ') was constructed at multiple times using (17) with the difference spectra in Fig. 2. Results are shown in Fig. 3. Streamfunction perturbations are obtained by solving the Poisson equation $\nabla^2 \psi' = \zeta'$. The solution to the Poisson equation is unique to within a constant value when using periodic boundary conditions. Therefore, the spatial mean $\langle \psi' \rangle$ was subtracted from each solution to ensure that the perturbation streamfunction remains unbiased.

As explained previously, error variances from the LAM simulation are greater than those of the global simulations for about the first 12 hours (see also Nutter et al., 2004). Therefore, the amplitude of vorticity perturbations are set to zero since the LAM simulation already has excessive error variance during this time. The impact of this choice is seen in Fig. 3a,b as the perturbation field does not begin to amplify until about 15 hours have passed. Careful examination of the vorticity perturbation field reveals about 10 to 20 wave couplets across the breadth of the 3000 km^2 domain. This result is consistent with the difference spectra shown in Fig. 2 since wavelengths are on the order of 150 to 300 km.

The vorticity field is translated at the Rossby phase velocity using (19) and (20). Motion from west to east is clearly evident in time animation of these fields, and is also seen in Fig. 3 by locating and tracking local minima and maxima. The translation and simultaneous amplification of the perturbation field is more easily seen in the streamfunction perturbations. Using the approximation $\Phi' = \psi' f$, note that the contours of ψ' correspond to $10 \text{ m}^2 \text{ s}^{-2}$ increments of geopotential height.

The vorticity and streamfunction perturbations fields are constructed at each time step, and at the spatial resolution of a LAM simulation. The perturbations are then added to the temporally interpolated LBC field provided by a coarsely-resolved external model simulation. This perturbed external LBC field is then blended with the LAM solution across the peripheral 7-point relaxation zone. The perturbations are produced as a field covering the entire LAM domain to ensure that the spatial variance is restored using coherent wave patterns. However, *the perturbations are applied only within the boundary zone and modify the LAM solution only after propagating into the domain.*

An example LAM ensemble obtained from simulations having perturbed LBCs is shown with its dispersion loss ratio (Eq. 11) in Fig. 4. The ‘‘spaghetti’’ contours and streamfunction dispersion (represented by the solid and dashed lines) appear much the same as in as in Fig. 1. Hence, the LBC perturbations have not introduced excessive noise into the individual ensemble member simulations.

The effects of the LBC perturbations for this example are seen in the dispersion loss ratio. During the first 12 to 24 hours, the dispersion loss ratio is similar in both perturbed and unperturbed simulations. This is expected since the amplitude of the perturbations is zero through the first 12 hours as discussed previously. Once the LBC perturbations begin to enter the LAM domain, they help enhance error variance locally and the dispersion loss ratio becomes less negative compared to the unperturbed simulation (Fig. 1). Comparison of the simulations after about 60 hours shows that LBC perturbations have swept through the domain. Regions of increased and decreased vorticity dispersion relative to the global simulation now appear evenly distributed throughout the domain. The LBC perturbations do not apply instantaneously across the breadth of the domain, but instead propagate inward to restore those scales that have been filtered out by LBC filtering and sweeping effects. After 96 hours,

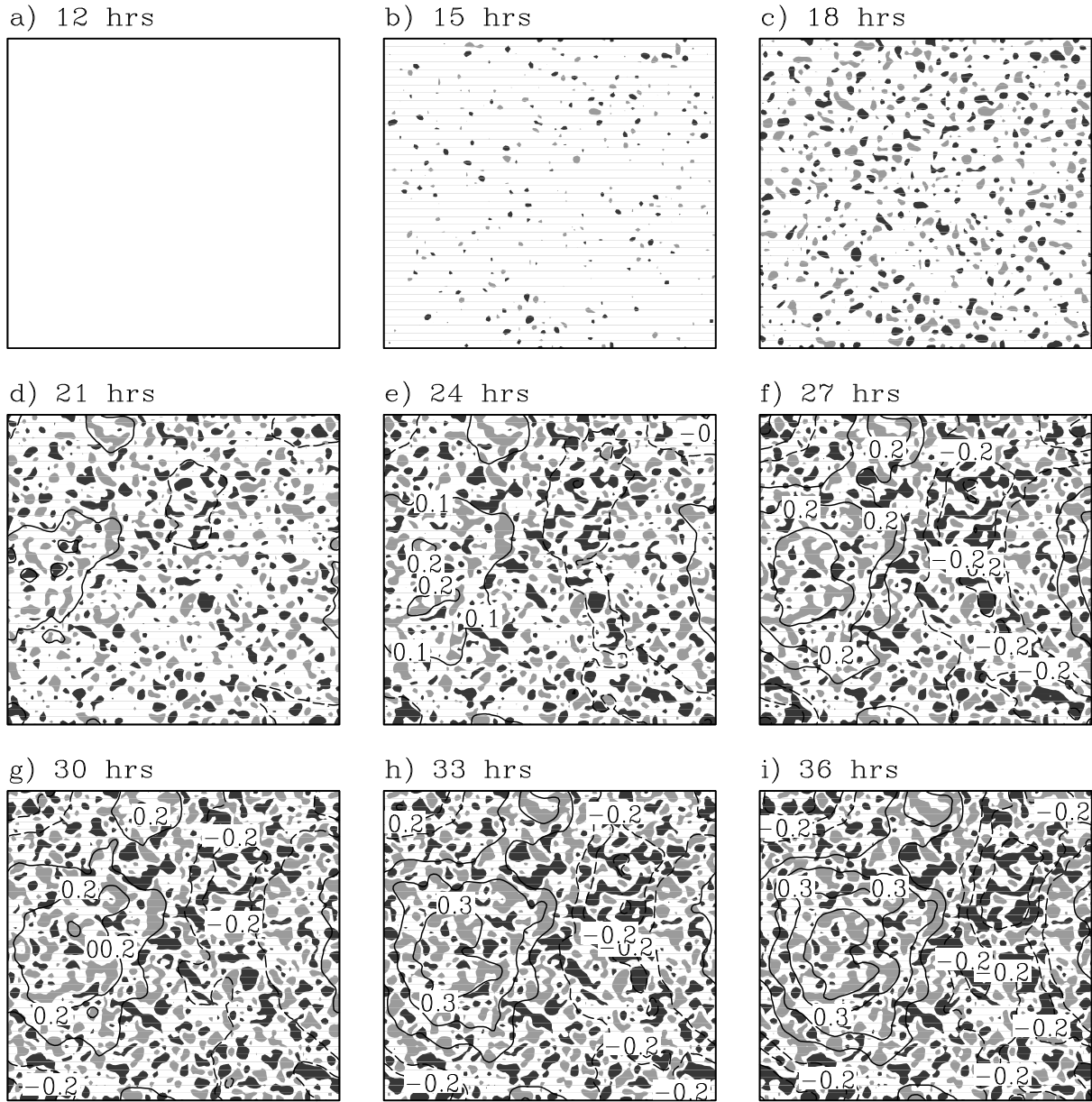


Figure 3: Example of LBC perturbation fields constructed for the medium domain using the difference in error variance spectra between global ensembles and LAM ensembles having 3-hourly updated, low-pass filtered LBCs (Fig. 2). Positive (negative) vorticity perturbations exceeding $0.5 \times 10^{-5} \text{ s}^{-1}$ are indicated by light (dark) shades. Positive (negative) streamfunction perturbations are shown with solid (dashed) contours at $\pm 0.1 \times 10^6 \text{ m}^2 \text{ s}^{-1}$ intervals (zero line omitted).

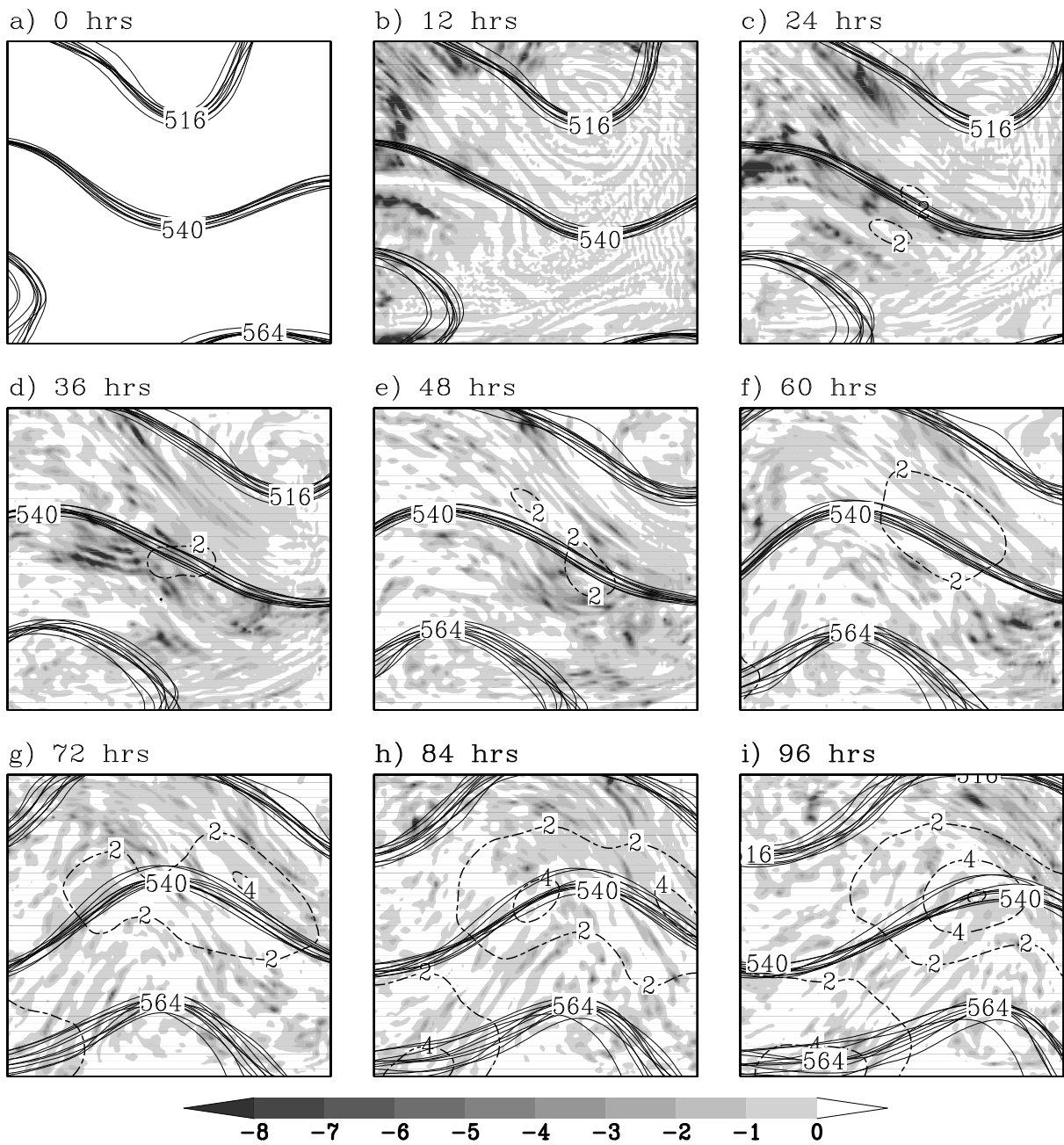


Figure 4: As in Fig. 1, except the example case is run with LBC perturbations such as those shown in Fig. 3.

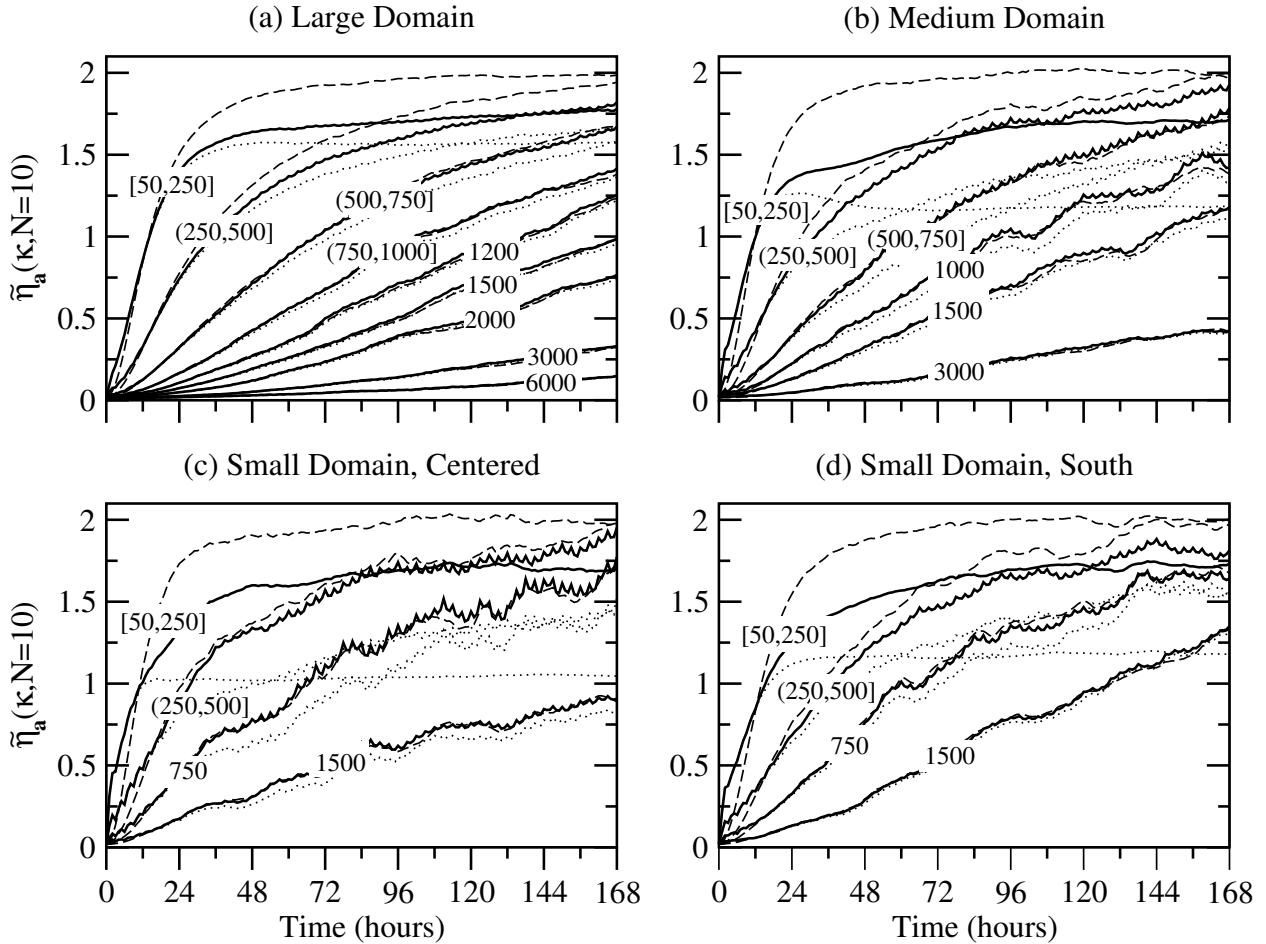


Figure 5: Normalized vorticity error variance (Eq. 9), averaged over 100 independent 10-member LAM ensemble simulations having perturbed, 3-hourly updated, low-pass filtered LBCs (150 km wavelength cutoff). Line labels (km) indicate wavelength(s) contributing to error variances. Dashed reference lines show error variances from subsets of global ensemble simulations and dotted lines show error variances from corresponding LAM ensemble simulations run without LBC perturbations.

the domain average dispersion loss ratio is -0.95 for the unperturbed simulation (Fig. 1i) and -0.11 for the perturbed simulation (Fig. 4i). Hence, the impact of the LBC perturbations has been to restore LAM ensemble dispersion from a loss of nearly 50% to a loss of just 10% relative to the global ensemble simulations.

6. Statistical Results

The LAM ensemble simulations run by Nutter et al. (2004) are repeated here, except LBC perturbations are created and applied at each time step during the simulations as discussed in the previous section. Statistical results are obtained as averages over 100 independent 10-member LAM ensemble simulations

and are compared to results obtained from the earlier unperturbed LAM simulations and also to those obtained from subsets of global model simulations.

a. Ensemble Error Variance Spectra

Consider results from the LAM ensemble configuration having 3-hourly updated, low pass filtered (coarsely resolved) LBCs that are perturbed at every time step. Normalized error variances shown in Fig. 5 reveal that the application of LBC perturbations completely restores error variances at wavelengths longer than about 500 km to values obtained from the control simulations run on the global domain. The LBC perturbations are less effective for smaller scales, where the proportion of error vari-

ance restored depends on domain size. For example, on the large domain (Fig. 5a), the LBC perturbations restore about 1/3 of the error variance lost at saturation in the smallest scales. Compare this to the small, centered domain (Fig. 5c), where the LBC perturbations restore more than 3/4 of the error variance lost in the unperturbed LAM simulations.

To explain these results, note that difference spectra used to determine the amplitude of LBC perturbations (Eq. 18) are based on error variance calculations obtained from data over the full extent of the LAM domain. However, LBC perturbations are applied only within the peripheral 7-point wave-absorbing zone. The perturbations subsequently disperse and/or dissipate while propagating through the LAM domain. Therefore, the difference spectra likely underestimate the amplitude of LBC perturbations needed to fully restore LAM error variances to those obtained from global simulations. The LBC perturbations are more effective on smaller domains because there is less time for dispersion and dissipation to reduce their impact while passing through the LAM domain. The perturbations also restore variance more effectively for larger scale waves since they have slower dispersion and less dissipation. Furthermore, the small-scale perturbations help maintain error variance at larger scales through nonlinear wave interactions and the upscale and downscale transfers of energy.

There are other interesting features seen in Fig. 5. First, note that variance spectra in the perturbed simulations are identical to those for unperturbed simulations over the first 12 to 24 hours. As discussed above, the amplitude of the perturbation field is set to zero during this time because the LAM variance spectra exceed those of the global simulations. Note also that the error variance curves continue to oscillate because of the LBC error “pulse” caused by temporal interpolation between otherwise perfect LBCs (see Nutter et al., 2004).

LAM simulations were also conducted after adding perturbations to hourly and 6-hourly updated LBCs (not shown). Normalized error variances (Eq. 9) obtained from simulations having perturbed, hourly updated LBCs (not shown) reveal that error variances from the perturbed LAM simulations are nearly superimposed with those from the laterally unbounded global ensemble simulations. This result shows that the LBC perturbations function as designed. However, the additional effort of applying LBC perturbations is not justified for hourly-updated LBCs since error growth constraints are minimal for this configuration (Nutter, 2003). Results from the LAM configuration having 6-hourly updated LBCs

(not shown) reveal similar features as those in Fig. 5, although the LBC perturbations are slightly less effective since they had a greater proportion of total variance to recover.

b. Ensemble Summary Statistics

It has been shown that the use of LBC perturbations capably restores much of the error variance lost by coarsely resolved and temporally interpolated external LBC fields, especially on smaller domains and at wavelengths longer than 250 km. The primary goal of applying LBC perturbations is to restore LAM ensemble dispersion without adversely impacting the individual ensemble members. Equation (8) provides a direct link between ensemble dispersion and the error variance evaluated in the previous subsection. It is useful to compare the relative magnitudes of each term in this equation to help determine what portion of total error variance (σ^2) contributes to ensemble dispersion (D^2) relative to the remaining bias terms. The ensemble mean square error (S^2 , Eq. 5) also is evaluated as an overall measure of performance.

Results are presented here for the model configuration having perturbed, 3-hourly updated, low-pass filtered (coarsely resolved) LBCs (Fig. 6). The loss of error variance at small scales due to LBC constraints was noted previously in Fig. 5. The integrated effect is a decrease in total error variance (σ^2) over the first 24-48 hours of the simulation, depending on domain size. In previous simulations without LBC perturbations, the loss of total error variance leveled off at a near constant value as LBC sweeping reached a balance with small-scale error growth on the interior of the LAM domain (see Nutter et al., 2004). In contrast, the amplitude of the LBC perturbations in the simulations shown here grow with time and begin to restore the total error variance. Consequently, the difference in spectra between global and LAM ensembles becomes less negative with time. The total error variance is not restored completely as noted in the previous section, but is most effectively restored on the smaller domains.

An interesting characteristic noted on all domains is the increase of total error variance in the LAM simulations during the first 12 hours. Close examination of Fig. 5 shows that this increase in variance is due to contributions at smaller scales. The source of this extra variance early in the LAM simulations is due to the different solution obtained by solving the Helmholtz equation to obtain vorticity from perturbed LBCs. This introduces the error variance at small scales, and also contributes to an increase in

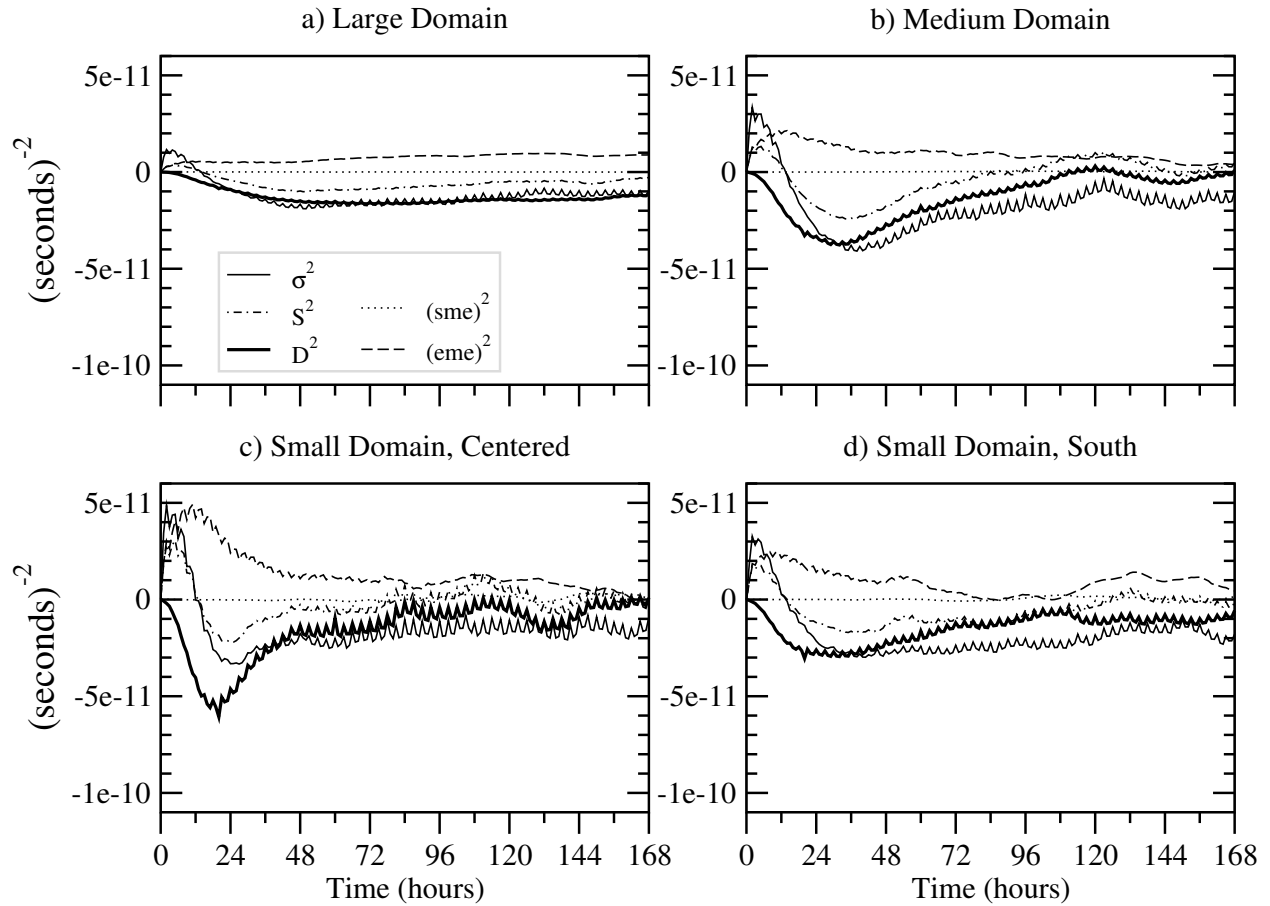


Figure 6: Difference in vorticity summary statistics for LAM ensemble simulations having perturbed, 3-hourly updated, low-pass filtered LBCs (150 km wavelength cutoff) compared to statistics from global ensemble simulations. Results are averaged over 100 independent 10-member ensemble simulations. Line labels in the legend are defined in section two.

ensemble mean error (Fig. 6). In spite of the initial increase in error variance, LAM ensemble dispersion decreases for about 48 hours in all simulations because of the increase in ensemble mean error in the absence of changes in the spatial bias (see Eq. 8).

The ensemble statistics oscillate with time due to the LBC error pulse caused by temporal interpolation. The oscillation has a 3-hour period associated with the interval at which LBCs are updated from external model fields. With each update, the external fields are perfect except for the removal of short waves by low-pass filtering to emulate coarse resolution and the subsequent addition of perturbations to restore variance at those scales.

The total error error variance is fully restored when LBC perturbations are applied in LAM configurations having hourly updated LBCs (not shown). This result is expected since error variance spectra

were restored at all wavelengths for this configuration (Nutter, 2003). Furthermore, the use of LBC perturbations does not introduce additional spatial bias or ensemble mean error. Most importantly, when using hourly updated LBCs, LAM ensemble dispersion is fully restored to values obtained from corresponding subsets of global ensemble simulations. Results from LAM configurations using 6-hourly simulations reveal similar results to those shown in Fig. 6.

7. Scaled LBC Perturbations

Results shown in Fig. 5 reveal that the amplitude of LBC perturbations needed to fully restore error variance growth is underestimated under certain LAM configurations. Specifically, the perturbation amplitudes are underestimated at wavelengths shorter than 500 km, especially when applied to large domain simulations having coarsely resolved external

LBCs updated at intervals of 3 hours or longer. In an attempt to remedy this deficiency, the perturbation amplitudes are increased by applying a scale factor to the difference spectra $|F'(k, l)|^2$ (Eq. 18). The scale factor is defined as ratio of error variances obtained from perturbed LAM ensembles to those obtained from corresponding subdomains of global ensemble simulations. Thus, the difference spectra are redefined by introducing the scaling factor Λ so that

$$\Lambda = \sigma_{\kappa}^2(\text{global}) / \sigma_{\kappa}^2(\text{perturbed LAM}) \quad (21)$$

and

$$|F'(k, l)|^2 = \Lambda[\sigma_{\kappa}^2(\text{global}) - \sigma_{\kappa}^2(\text{unperturbed LAM})]. \quad (22)$$

The use of scaled LBC perturbations does yield a small improvement for the LAM configuration having low-pass filtered LBCs that are updated every 3-hours (not shown). Given an increase in perturbation amplitudes of up to 40% after scaling, the increase in error variance at scales less than 500 km is about 0 to 6%. Although tiny improvements are seen in the error variance spectra, the ensemble summary statistics (not shown) indicate that ensemble dispersion is almost unchanged compared to the configuration having unscaled LBC perturbations. Hence, the significance of these improvements using scaled LBC perturbations is questionable and not recommended given the additional computational expense.

8. Conclusions

A new method has been developed to apply LBC perturbations at every time step of LAM simulations. The perturbations are intended to restore the small-scale error variances and ensemble dispersion lost due to coarsely resolved and temporally interpolated external LBC fields.

Results showed that the application of LBC perturbations in LAM ensemble simulations is highly effective at restoring error variances and ensemble dispersion to the values obtained from subsets of global ensemble simulations. Two exceptions were noted. First, error variances were not fully restored at wavelengths shorter than 500 km, especially for large domain simulations having coarsely resolved external LBC fields updated at intervals of 3 hours or longer. This deficiency was attributed to the fact that short-wavelength LBC perturbations have small amplitudes and subsequently disperse and/or dissipate while propagating through the LAM domain. The second notable exception is that, in spite of the gain in error variance, ensemble dispersion for the small domains could not be fully recovered between

about 12 and 48 hours of the simulations. This deficiency was explained by the increase in ensemble mean error caused by coarsely resolved and temporally interpolated external LBC fields. The increase in ensemble mean error causes a decrease in ensemble dispersion that cannot be recovered by the use of LBC perturbations as applied herein.

The LBC perturbations are based solely on differences in error variance spectra. Their only relationship to the dynamical evolution of flow inside the LAM domain is through the nonlinear advection term that transfers energy and enstrophy upscale and downscale throughout the spectrum. To ensure that the LBC perturbations do not overwhelm the quality of the LAM solution, it is necessary that their amplitudes remain small. Furthermore, the ensemble mean error can become inflated if the perturbations are too strong. An increase in ensemble mean error contributes to a loss of ensemble dispersion, which opposes the effort to restore dispersion through increases in error variance. Although not perfect in every aspect, the LBC perturbations developed in this work appear small enough to satisfy these concerns while restoring most of the ensemble dispersion and error variance lost through LBC constraints.

We conclude with comments on how this work may apply to more realistic modeling systems. Two fundamental assumptions were made at the start of this work (Nutter et al., 2004). First, it was assumed that natural error growth at large scales is (or can be) stated accurately using global model forecasts. This assumption is needed to ensure that error variances and ensemble dispersion are correct at wavelengths exceeding the breadth of the LAM domain. LBC perturbations are only effective at scales up to the size of the LAM domain and cannot correct deficiencies caused by improper error growth rates at larger scales. Second, the assumption was made that error growth rates at small scales in LAMs should behave the same as those in global models operating at equivalent resolution. The amplitude of the LBC perturbations was determined by the difference in error variance spectra between global ensembles and LAM ensembles having unperturbed LBCs. Hence, the LBC perturbations may be less effective if there are differences in the variance spectra caused by dynamical or artificial discrepancies between external and LAM models. A related assumption is that the model simulations are unbiased, since ensemble dispersion is linked to the total error variance, the ensemble mean error and the spatial bias. This secondary assumption is less important because corrections can be applied for systematic model errors.

The greatest challenge faced in applying the LBC perturbation technique to other modeling systems is the determination of appropriate amplitude coefficients needed for constructing the perturbation fields. Global ensemble systems have been available for more than a decade. It should not be difficult to obtain error variance spectra over many cases for these ensembles, especially since most are integrated using spectral methods. The greater challenge is to obtain error variance spectra from LAM ensemble systems. LAM ensemble systems have existed for several years, but most do not include the statistical verification packages needed to calculate one-dimensional error variance spectra. Such packages would need to be developed, then results accumulated over many cases. Once an appropriate set of verification data has been accumulated, corrections for systematic errors must be applied before obtaining difference spectra. Finally, an issue that requires additional research is how to determine the vertical structure of LBC perturbations.

Temporal interpolation of coarsely resolved external LBC fields has been shown to remove small-scale features from LAM solutions and quickly sweep out any set of initial condition perturbations (Nutter et al., 2004). LBC perturbations applied at every time step are essential to the design of an efficacious LAM ensemble system. The effort will be most rewarding on smaller domains where LBC sweeping effects act most quickly to constrain error growth rates. The additional expense of applying LBC perturbations may be offset by the ability to integrate LAM ensembles over smaller domains.

Acknowledgement

This research was supported by funding from several sources: the University of Oklahoma (OU) School of Meteorology through the Robert E. Lowry endowed chair; the Department of Defense of the U.S.A. under grant N00014-96-1-1112, or Coastal Meteorology Research Program (CMRP); the Williams Energy Marketing and Trading Company through a Williams Graduate Research Fellowship within the OU Center for Analysis and Prediction of Storms (CAPS); the National Science Foundation under grant ATM-0129892, related to the International H₂O Project (IHOP); and the OU Alumni Association Fellowship Program.

The National Severe Storms Laboratory (NSSL) shared desk space and access to a multiprocessor computer. The OU School of Meteorology provided excellent infrastructure and administrative support. Most of the computations were performed on the

IBM Regatta p690 symmetric multiprocessor computer operated by the OU Supercomputing Center for Education and Research (OSCER).

References

- Dalcher, A. and E. Kalnay, 1987: Error growth and predictability in operational ecmwf forecasts. *Tellus*, **39A**, 474–491.
- Davies, H. C., 1976: A lateral boundary formulation for multilevel prediction models. *Quart. J. Roy. Meteor. Soc.*, **102**, 405–418.
- 1983: Limitations of some common lateral boundary schemes used in regional NWP models. *Mon. Wea. Rev.*, **111**, 1002–1012.
- De Elía, R. and R. Laprise, 2002: Forecasting skill limits of nested, limited-area models: A perfect-model approach. *Mon. Wea. Rev.*, **130**, 2006–2023.
- Errico, R. M., 1985: Spectra computed from a limited area grid. *Mon. Wea. Rev.*, **113**, 1554–1562.
- Errico, R. M. and D. Baumhefner, 1987: Predictability experiments using a high-resolution limited-area model. *Mon. Wea. Rev.*, **115**, 488–504.
- Hamill, T. M., 2001: Interpretation of rank histograms for verifying ensemble forecasts. *Mon. Wea. Rev.*, **129**, 550–560.
- Hamill, T. M. and S. J. Colucci, 1997: Verification of Eta-RSM short-range ensemble forecasts. *Mon. Wea. Rev.*, **125**, 1312–1327.
- Holton, J. R., 1979: *An Introduction to Dynamic Meteorology*, volume 23 of *International Geophysics Series*. Academic Press, 2nd edition.
- Hou, D., E. Kalnay, and K. K. Droegemeier, 2001: Objective verification of the SAMEX '98 ensemble forecasts. *Mon. Wea. Rev.*, **129**, 73–91.
- Laprise, R., M. R. Varma, B. Denis, D. Caya, and I. Zawadzki, 2000: Predictability of a nested limited-area model. *Mon. Wea. Rev.*, **128**, 4149–4154.
- Leith, C. E., 1974: Theoretical skill of Monte Carlo forecasts. *Mon. Wea. Rev.*, **102**, 409–418.
- Lorenz, E. N., 1982: Atmospheric predictability experiments with a large numerical model. *Tellus*, **34**, 505–513.

- Nutter, P., 2003: *Effects of Nesting Frequency and Lateral Boundary Perturbations on the Dispersion of Limited-Area Ensemble Forecasts*. Ph.D. dissertation, University of Oklahoma.
- Nutter, P., D. Stensrud, and M. Xue, 2004: Effects of coarsely-resolved and temporally-interpolated lateral boundary conditions on the dispersion of limited-area ensemble forecasts. *Submitted to Mon. Wea. Rev.*, **132**, xxxx–xxxx.
- Paegle, J., Q. Yang, and M. Wang, 1997: Predictability in limited area and global models. *Meteorol. Atmos. Phys.*, **63**, 53–69.
- Press, W. H., S. A. Teukolsky, W. T. Vetterling, and B. P. Flannery, 1996: *Numerical Recipes in Fortran 77: The Art of Scientific Computing*. Cambridge University Press, 2nd edition.
- Reynolds, C. A., P. J. Webster, and E. Kalnay, 1994: Random error growth in NMC's global forecasts. *Mon. Wea. Rev.*, **122**, 1281–1305.
- Schubert, S. D. and M. Suarez, 1989: Dynamical predictability in simple general circulation model: Average error growth. *J. Atmos. Sci.*, **46**, 353–370.
- Stroe, R. and J. F. Royer, 1993: Comparison of different error growth formulas and predictability estimation in numerical extended-range forecasts. *Ann. Geophysicae*, **11**, 296–316.
- Vukicevic, T. and R. M. Errico, 1990: The influence of artificial and physical factors upon predictability estimates using a complex limited-area model. *Mon. Wea. Rev.*, **118**, 1460–1482.
- Walker, J. S., 1988: *Fourier Analysis*. Oxford University Press.
- Warner, T. T., R. A. Peterson, and R. E. Treadon, 1997: A tutorial on lateral boundary conditions as a basic and potentially serious limitation to regional numerical weather prediction. *Bull. Amer. Meteor. Soc.*, **78**, 2599–2617.